Sweep System Design for a Heavy Ion Beam Probe on MST

Jianxin Lei

ECSE Department, Rensselaer Polytechnic Institute, Troy, NY 12180

(June 28, 1998)

The sweep system for the HIBP (Heavy Ion Beam Probe) on the Madison Symmetric Torus is described. The two components of the system are the primary sweep optics and secondary collimation plates. Key issues in the sweep system design are the small entrance and exit ports available on MST, the significant toroidal beam motion induced by the strong poloidal magnetic field and the excessive current loading due to plasma and UV. The design accommodates these issues using a crossover sweep plate design in two dimensions for the primary beam as well as two dimensional sweeping on the secondary beam. The primary beam sweep design results in a sweep range of $\pm$ 20 degrees in one direction and $\pm$ 5 degrees in the perpendicular direction. The secondary beam sweep design results in entrance angles to the energy analyzer of < 3 degrees in radial and $\sim$ zero degree in toroidal directions. The procedure for calculating sweep performance including fringe fields, a system for active trajectory control, and initial experiments on plasma and UV loading are also discussed.

Contents

I. INTRODUCTION

A heavy ion beam probe measures a variety of plasma parameters in magnetically confined plasmas, including the electrostatic potential profile, potential and density fluctuations, and the magnetic field[1]. These parameters are important for RFP research in anomalous transport, magnetic equilibrium, current profile modifications, and instability studies[2].

In an HIBP experiment, a singly charged ion beam (the primary beam) is injected into the plasma. As the beam passes through the plasma, doubly charge ions (the secondary beam) are created. Only those secondaries created in a relatively small sample volume determined by a detector aperture are measured. Information about the electron density, electric potential, and magnetic field is contained in the secondary beam intensity, energy, and toroidal deflection.

The sample volume position is controlled by changing the entrance angle of the beam to the plasma using electrostatic sweep plates. Design of TEXT-HIBP was briefly reviewed in reference 1.

The MST HIBP requires novel design features in order to reach the desired sample volumes and they are the subject of this paper. The principle reason for the complication is the small ports available on MST. The MST vacuum vessel also acts essentially as a coil system carrying large currents. Large ports would perturb the vacuum chamber currents and are therefore not allowed. Hence the HIBP experiment will use a 5 cm diameter entrance port and a 11.4 cm diameter exit port. These are substantially smaller than ports on previous experiments.

In an idealized case, the HIBP is modeled as having all trajectories originate from a sweep point. With small ports, this sweep point is forced to be much closer to the port than normally. This in turn, results in a large required sweep angle range and increased exposure of the sweep plates to UV radiation and plasma streaming out of the port. Similar constraints will also affect the NSTX-HIBP design[3].

A large angular range is present on both the primary and secondary beamlines. The secondary beam angular range is larger than can be accommodated by the energy analyzer used to determine beam energy. Therefore, a secondary sweep system will also be required. Secondary sweep plates have been used on T10-HIBP[4] and CHS-HIBP[5,6], but have never been used on Rensselaer HIBPs.

Finally, the sweep system design is complicated due to the fact that the poloidal and toroidal magnetic fields have comparable strengths. This results in a fully 3-dimensional trajectory and sweep systems with significant requirements in 2 dimensions. The design model and the results of the primary and secondary sweep system designs are described in the next section. Control of those trajectories to reach core or edge regions is discussed in section 3. Initial plasma/UV loading tests have been done on MST and are discussed in section 4. Conclusions and future work are discussed in section 5.

II. DESIGN OF THE SWEEP SYSTEMS

A. Design Model

With one pair of sweep plates, the ion beam velocity and position are both changed. This makes it difficult to get a large range of angles through a small port. Figure 1 shows a schematic of a 1 dimensional cross-over sweep system that can be used to get a large angular range through a small port. This is the approach used in this design.
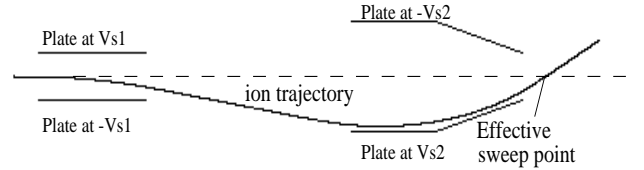

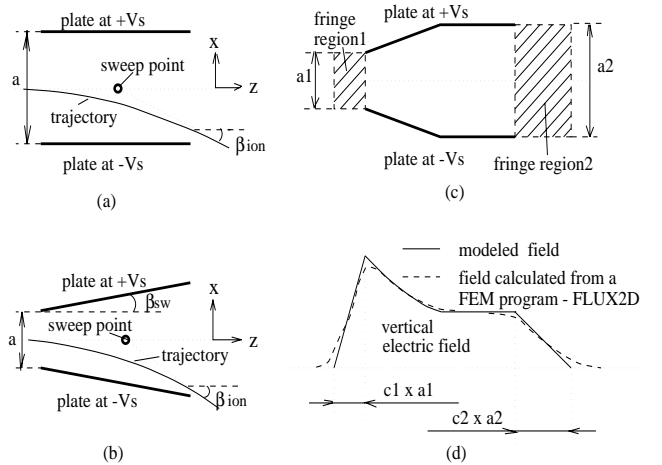FIG. 1. Illustration of 1-D crossover sweep

FIG. 2. Illustration of sweep plates: parameters and geometry (a) Straight plates; (b) Flared plates; (c) A combined plates and an illustration of fringe fields model; (d) Illustration of field distribution of case (c)

The various elements of the sweep system can be modeled as combinations of the elements shown in Fig. 2(a) and (b). The simplest model assumes that the electric field is uniform in the straight plates region and zero outside, while the electric field in the flared region can be modeled using the average vertical component of the field at a given position and neglecting other field components[7]. Mathematically, this can be analyzed using the ion optics transfer matrices below for the straight and flared regions respectively (See appendix A):

$$\begin{bmatrix} x \\ \frac{dx}{dz} \end{bmatrix} = \begin{bmatrix} 1 & z \\ 0 & 1 \end{bmatrix} \begin{bmatrix} x_0 \\ \frac{dx}{dz}\big|_0 \end{bmatrix} - f\frac{z}{a} \begin{bmatrix} z/2 \\ 1 \end{bmatrix} \qquad (1)$$

$$\begin{bmatrix} x \\ \frac{dx}{dz} \end{bmatrix} = \begin{bmatrix} 1 & z \\ 0 & 1 \end{bmatrix} \begin{bmatrix} x_0 \\ \frac{dx}{dz}\big|_0 \end{bmatrix} - \frac{f}{k} \ln\left(1 + \frac{kz}{a}\right) \begin{bmatrix} \frac{a}{k} + z \\ 1 \end{bmatrix}$$
$$+ \frac{fz}{k} \begin{bmatrix} 1 \\ 0 \end{bmatrix} \tag{2}$$

where x_0 and $dx/dz|_0$ are position and slope at the entrance to a region, z is horizontal length of a region, $f = qV_s/W_b$ represents deflecting strength of the plates, q is ion charge in unit of e, W_b is ion beam energy in unit of eV, V_s is the sweep plate voltage in unit of *volt*, and $k = 2\tan(\beta_{sw})$, is the slope of the plates. For a drift region, set $f = 0$ in eq.(1).

The fringe field is neglected in the model above, and $W_b = m_i v^2/2 = const.$ is assumed. In previous experiments, this model has had errors of roughly 10-20%[1]. Although the analytical solution of the electric field including fringe fields can be found, a transfer matrix describing the ion trajectory has not been found. Instead, a simple modified model is used to take fringing effects into account. As shown in fig. 2(c) and (d), the modified model assumes that the electric field in the plate region has the same form as before, but linearly drops to zero outside the plates over a distance given by $c_1 * a_1$ or $c_2 * a_2$. c_1 and c_2 are dimensionless coefficients, and their values have been set by examining 2-D numerical solutions to Laplace eq. Typical values are 1 for large b/a (*e.g.* > 1.5), and smaller (*e.g.* 0.8) for $b/a \simeq 1$.

The ion trajectory in the front and back fringe regions are decided by the following equations respectively (See appendix B):

$$\begin{bmatrix} x \\ \frac{dx}{dz} \end{bmatrix} = \begin{bmatrix} 1 & z \\ 0 & 1 \end{bmatrix} \begin{bmatrix} x_0 \\ \frac{dx}{dz}\big|_0 \end{bmatrix} - f\frac{z^2}{2a_1^2} \begin{bmatrix} z/3 \\ 1 \end{bmatrix} \tag{3}$$

$$\begin{bmatrix} x \\ \frac{dx}{dz} \end{bmatrix} = \begin{bmatrix} 1 & z \\ 0 & 1 \end{bmatrix} \begin{bmatrix} x_0 \\ \frac{dx}{dz}\big|_0 \end{bmatrix} - \frac{fz}{a_2} \begin{bmatrix} z/2 \\ 1 \end{bmatrix} + \frac{fz^2}{2a_2^2} \begin{bmatrix} z/3 \\ 1 \end{bmatrix} \tag{4}$$

where parameters have the same meanings as before. The calculation error with the modified model is reduced to below 5%. Equations (1)-(4) are used to determine the system design and the required sweep voltages.

B. Primary Sweep System

Primary sweep plates are used to control the angle at which the primary beam enters the plasmas magnetic field. According to our MST-HIBP trajectory calculations, the required sweep angle ranges are $\sim \pm 20°$ radially and $\sim \pm 5°$ toroidally. This is several times larger than on previous systems. Crossover sweep is needed because of the small port. Fig. 3(a) is a schematic view of the primary sweep system that has been designed using the transfer matrix technique. Note that all directions in the figure have same scale. Not shown are guard rings at

the sides of some sweep plates to compensate for fringe field effects there. Two pairs of sweep plates are used in each direction in order to obtain a 2-D crossover sweep. This moves the effective sweep point beyond the ends of plates. The design is able to steer a 200 keV ion beam over the required angular ranges. 200 kV is the maximum accelerator voltage available although most experiments will operate at lower voltages. Existing 20, 10, and 4 kV power supplies with fast slew rates will be used to power the sweep plates. The system is designed to be as compact as possible and has a total length of ~ 110 cm. The distance between the plasma and the front plates is 10 cm. The 5 cm thick vacuum chamber and hardware to reduce plasma loading will be in this 10 cm region. The mechanical support structure for the plates is under design now. To increase flexibility, the system will be rotatable around the beamline to get the best combined radial/toroidal angles for a given experiment and it will also be movable along the beamline to reduce the plasma/UV loading effect.

(a) Primary sweep plates
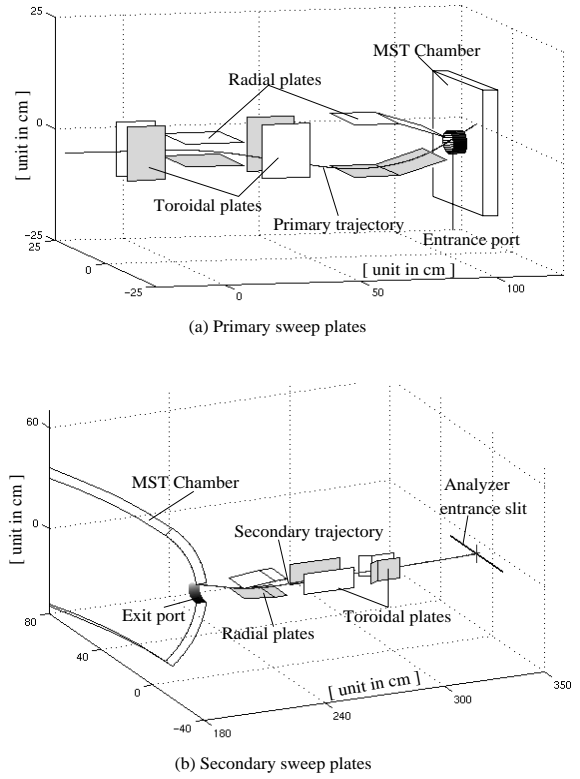

(b) Secondary sweep plates

FIG. 3. Schematic view of the sweep system designed

Appendix E shows some simulation results by using guard rings to reduce side fringing effects.

Appendix F descirbes the parameters and geometry of the primary sweep plates designed.

C. Secondary Sweep System

In past RPI beam probes, the energy analyzer was located at the detection point decided by a trajectory program. Although the analyzer is designed so that it is insensitive to the beam entrance angle in the vertical (*i.e.* radial or poloidal) direction, it is desirable to limit the entrance angle variation to less than $\pm 5°$. Furthermore, it is critical to keep the horizontal entrance angle less than $1°$. The angular range at the detection point in the calculations is much larger than those of past HIBPs because of the small ports. In addition, the MST magnetic field which has comparable B_t and B_p results in large toroidal (horizontal) entrance angles. Simply moving the analyzer away from the plasma would reduce the entrance angle range, but this would result in an unacceptably small number of sample volume locations. A secondary sweep system has been designed that reduces the beam entrance angle & positions to acceptable values. It has the further advantage of placing the analyzer further from the plasma which will reduce its UV loading.

Figure 3(b) shows the secondary sweep system. As with the primary sweep system, the design can steer a beam over the full desired angle range for a 200 keV ion beam and utilizes existing power supplies. Total length of the sweep system is ~ 80 cm resulting in an analyzer location that is 140 cm away from the exit port. The first set of plates, powered by 10 kV supplies, steers the beam in the radial (vertical) direction and changes the incident angle range from $\pm 17°$ to $\pm 3°$ at the analyzer entrance slit. The 2nd and 3rd sets of plates use 4 kV power supplies and a crossover type design to steer the beam so that it enters the analyzer on the horizontal (toroidal) midplane with 0 toroidal angle. The incident angle range without sweep plates is $\pm 5°$. The mechanical support system for the plates is being designed and will also be rotatable and translatable to increase flexibility.

Despite the wide angle range handled by this design, it still cannot look at all possible sample volume positions with a single analyzer position. Therefore, the secondary beamline is being designed with the possibility of changing analyzer locations by pivoting the beam line. Two beamline orientations that are optimized for edge ($r/a > 0.5$) and core ($r/a < 0.5$) are shown in Fig. 4.
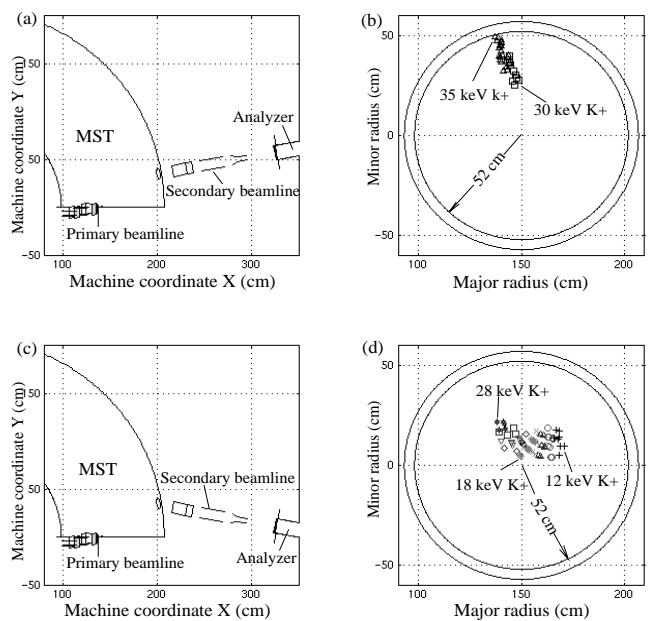

FIG. 4. Top views of the beamline arrangements and their observation points: (a) and (b) for edge diagnostics; (c) and (d) for core diagnostics

Appendix G descirbes the parameters and geometry of the secondary sweep plates designed.

III. ACTIVE TRAJECTORY CONTROL

In order to look at multiple sample volumes within a single shot, it will be necessary to control the sweep voltages on all sweep plates simultaneously. The various sweep voltages are set by 4 independent parameters. On CHS, such an active trajectory control system was implemented using results from trajectory calculations[5]. In that case, the fields in the helical plasma were well known and only slightly changed due to the presence of the plasma. However, in MST, the plasma generated magnetic fields dominate and are only partially known. Hence, we expect that our initial operation will involve running multiple trajectories for a few plasma conditions until a database is built up with sample volume locations and sweep voltages. Accuracy will be improved by iterating experimental results and trajectory simulations. Ultimately, active trajectory control like that achieved on CHS is the goal.

Appendix C and D show examples of how to decide the voltages on the secondary sweep plates once we know incident conditions.

Appendix H describes trajectory calculations in the sweep system and MST plasma.

Appendix I describes one effort searching for optimal position of the secondary beamline and some results.

4

IV. PLASMA/UV LOADING EFFECTS AND MITIGATION TECHNIQUES

The sweep plates design assumes there is no charge between the plates. This is basically true for previous experiments because the sweep plates were located far away from the ports. It will be more difficult to achieve this on MST. The primary sweep plates will be as close as 5 cm away from the 5 cm entrance port, and the secondary sweep plates will be ~ 20 cm away from the 11.4 cm exit port. There are two sources of electric charges in the sweep region. The first is plasma diffusion through the vacuum chamber port. A rough estimate suggests that n_e can be as high as $10^{11} \sim 10^{12}/cm^3$ just outside the port. The second source of charge is photo-electrons generated when UV photons strike the sweep plates. These electrons can create a plasma between the plates that leads to voltage breakdown and an electrical short if the power supply current limits are exceeded. A series of loading tests have been conducted on MST to identify possible problems. Figure 5 shows one of our test structure and current vs.voltaage results with/without magnets mitigation technique.
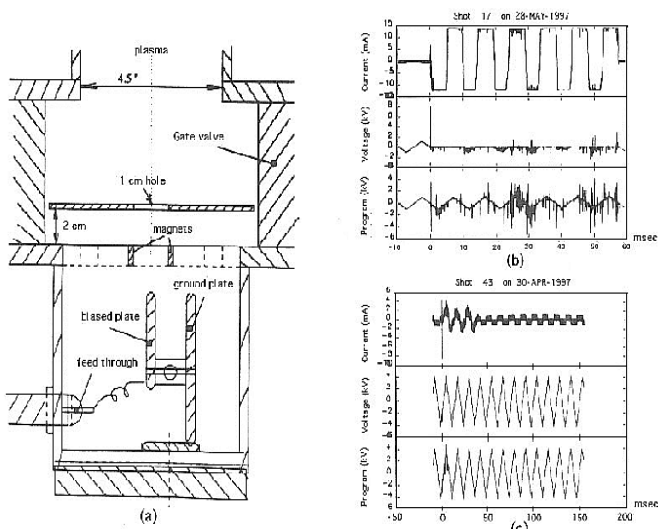

FIG. 5. Plasma/UV loading test structure and results: (a) Test structure; (b) Results without magnets; (c) Results with magnets

Results show that loading is plasma dominated. A magnetic field (~ 0.15 T.) applied normal to the beamline at a position between the test plates and the port reduced plasma loading substantially as would be expected if the loading was due to plasma. Since the effective sweep points are located between the plates and the ports, the range of beam positions is limited in this region and it is not difficult to place permanent magnets close enough to each other to reduce the plasma loading while simultaneously not obstructing the diagnostic beam. This magnet structure is currently being designed. In another test, a mesh screen was placed between the plates and the port.

The grid was fairly coarse with a spacing much greater than the Debye length ($\lambda_D \sim 0.1mm$). Nevertheless, it also showed a noticeable reduction in loading. A mesh as part of the final HIBP design will require high transparency ($> 90\%$) which will conflict with the ability to effectively screen out the plasma. We plan to initially use permanent magnets, but will keep a mesh screen as an option.

V. CONCLUSIONS AND FUTURE WORK

Primary and secondary sweep systems for the MST HIBP have been designed using a transfer matrix method. A simple model has been introduced to deal with fringe field of the sweep plates. Crossover design of the sweep plates moves the effective sweep points to the positions between the plates and the ports, which is necessary with the small MST ports. The primary sweep system designed provides $\pm 20°$ radial and $\pm 5°$ toroidal sweep ranges, which enable the ion beam to cover a large area of the plasma. The secondary beam sweep system has been designed to handle the large emittance from the exit port, and reduce the angular range and beam location at the analyzer to acceptable values. The analyzer location is also moved away from the exit port.

Experiments have shown that plasma loading is the dominant loading effect on the sweep plates, and that magnetic fields can suppress this effect. Other mitigation techniques are also being considered.

Two elements of the system design that still must be completed are the sweep plate support structure and the arrangement of permanent magnets to reduce plasma loading on the plates. In addition, further tests of mitigating structures are planned in the near term.

Once the system is operational, we eventually would like to use active trajectory control to scan the plasma. In order to do this, a combination of experimental data, sweep system calculations using equations (1) - (4), and trajectory simulations in the plasma will be used to build a database of sweep voltages and sample volume positions. This will be repeated for several different plasma configurations.

Appendix J describes how to determine the positions and size of those magnets mitigation structures beyond the end of primary sweep plates and in front of the secondary sweep plates.

[1] T. P. Crowley, IEEE Trans. on Plasma Sci., **22**(4), 291 (1994)

[2] U. Shah, K. A. Connor, J. Lei, P. M. Schoch, T. P. Crowley, and J. Schatz, Rev. Sci. Instrum., to be published.

[3] F. H. Mull, T. P. Crowley, P. M. Schoch, and K. A. Connor, Rev. Sci. Instrum., to be published.

[4] A. V. Melnikov, K. N. Tarasyan, V. A. Vershkov, V. A. Dreval, A. A. Sushkov, S. E. Lysenko, V. V. Sannikov, A. V. Gorshkov, L. I. Krupnik, I. S. Nedzelskij, N. K. Kharchev, G. A. Fomin, and L. A. Mochalova, IEEE Trans. on Plasma Sci., **22**(4), 363 (1994)

[5] A. Fujisawa, H. Iguchi, S. Lee, T. P. Crowley, Y. Hamada, and S. Hidekuma, Rev. Sci. Instrum. **67**(9), 3099 (1996)

[6] A. Fujisawa, H. Iguchi, M. Sasao, Y. Hamada, and J. Fujita, Rev. Sci. Instrum. **63**(7), 3694 (1992)

[7] John Mathew, Ph.D thesis, Rensselaer Polytechnic Institute, Dec. 1984

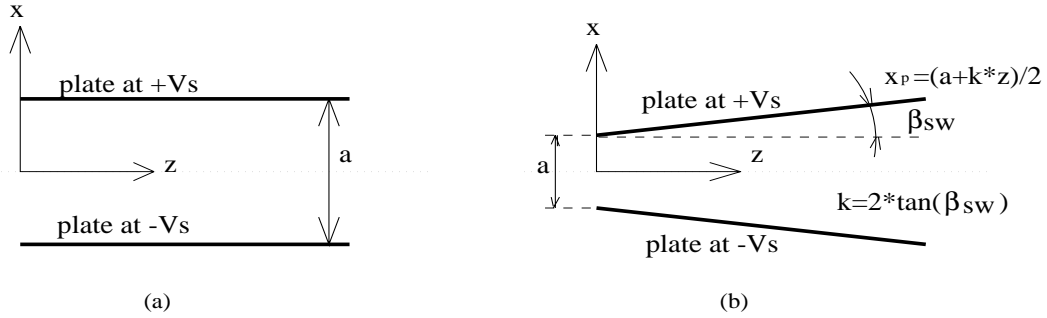## A. Trajectory equations in the straight and flared plates regions

FIG. 6. Elements of sweep plates: (a) straight plates; (b) flared plates

For the trajectory in the straight plates, if the coordinate for our calculation is like that shown in figure 6(a), we can derive the trajectory equation as following:

$$\ddot{x} = \frac{d^2 x}{dt^2} = -\frac{2qV_s}{m_i a} = \frac{d^2 x}{dz^2} \cdot \left(\frac{dz}{dt}\right)^2 = \frac{d^2 x}{dz^2} \cdot \frac{2W_b}{m_i}$$

$$\Rightarrow \frac{d^2 x}{dz^2} = -\frac{qV_s}{W_b a}$$

$$\Rightarrow \frac{dx}{dz} = -\frac{qV_s}{W_b a} \cdot z + \left.\frac{dx}{dz}\right|_0 \tag{5}$$

$$\Rightarrow x = -\frac{qV_s}{2W_b a} \cdot z^2 + \left.\frac{dx}{dz}\right|_0 \cdot z + x_0 \tag{6}$$

where q is the ion charge state, W_b is the beam energy in unit of keV, V_s is voltage on one plate in unit of kV. If define $f = qV_s/W_b$, eqs. (5) and (6) just give us equation (1). In the above, $dz/dt = const.$ is assumed.

For the trajectory in the flared plates, if the coordinate for our calculation is like that shown in figure 6(b), we can derive the trajectory equation as following:

Assume the electric field in the flared region only has vertical component E_x, and

$$\mathbf{E} = E_x \hat{a}_x = -\frac{2V_s}{2x_p}\hat{a}_x = -\frac{2V_s}{a + kz}\hat{a}_x$$

then

$$\ddot{x} = \frac{d^2 x}{dt^2} = -\frac{2qV_s}{(a + kz)m_i} = \frac{d^2 x}{dz^2} \cdot \left(\frac{dz}{dt}\right)^2 = \frac{d^2 x}{dz^2} \cdot \frac{2W_b}{m_i}$$

$$\Rightarrow \frac{d^2 x}{dz^2} = -\frac{qV_s}{W_b(a + kz)}$$

$$\Rightarrow \frac{dx}{dz} = \left.\frac{dx}{dz}\right|_0 - \frac{f}{k}\ln(a + kz) + \frac{f}{k}\ln(a) = \left.\frac{dx}{dz}\right|_0 - \frac{f}{k}\ln\left(1 + \frac{kz}{a}\right) \tag{7}$$

$$\Rightarrow x = x_0 + \left.\frac{dx}{dz}\right|_0 \cdot z - \frac{f}{k}\frac{a}{k}\left\{\left(1 + \frac{kz}{a}\right)\ln\left(1 + \frac{kz}{a}\right) - \left(1 + \frac{kz}{a}\right)\right\}\Bigg|_0^z$$

$$\Rightarrow x = x_0 + \left.\frac{dx}{dz}\right|_0 \cdot z - \frac{fa}{k^2}\left(1 + \frac{kz}{a}\right)\ln\left(1 + \frac{kz}{a}\right) - \frac{fa}{k^2}\left(-\frac{kz}{a}\right)$$

$$\Rightarrow x = x_0 + \left.\frac{dx}{dz}\right|_0 \cdot z - \frac{f}{k}\left(\frac{a}{k} + z\right)\ln\left(1 + \frac{kz}{a}\right) + \frac{fz}{k} \tag{8}$$

where $f = qV_s/W_b$ is known, and eqs. (7) and (8) just give us equation (2).

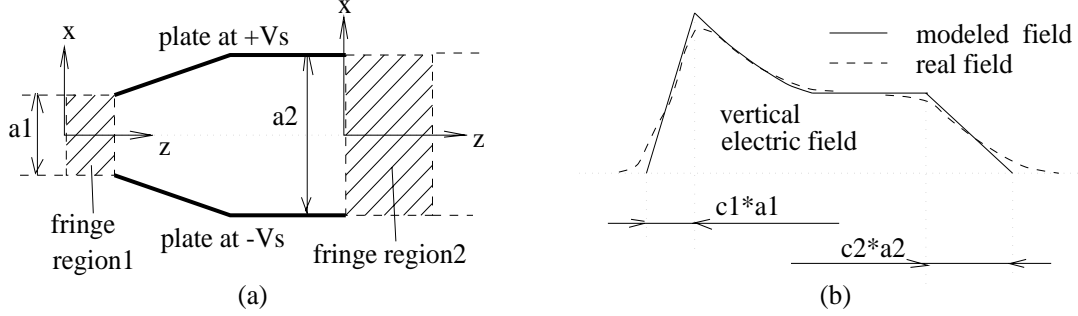## B. Trajectory equations in the fringe regions

FIG. 7. Elements of fringe regions: (a) illustration of fringe regions ; (b) illustration of fringing field distribution

There are two kinds of fringe regions used in our modified model, as that shown in figure 7(a), both refer to the ion trajectory. The 1st is the region that the electric field (only consider vertical component seen by the ion) changes from zero to the full scale, corresponding to the case that the ion passes from the left into the fringe region1 to the right into the plates region. The vertical electric field felt by the ion is like that shown in figure 7(b), where the vertical field can be simplified as:

$$E_x = \frac{2V_s}{a_1} \cdot \frac{z}{c_1 a_1}$$

We can derive the trajectory from above simplification:

$$\ddot{x} = \frac{d^2 x}{dt^2} = -\frac{2qV_s}{m_i a_1} \cdot \frac{z}{c_1 a_1} = \frac{d^2 x}{dz^2} \cdot \left(\frac{dz}{dt}\right)^2 = \frac{d^2 x}{dz^2} \cdot \frac{2W_b}{m_i}$$

$$\Rightarrow \frac{d^2 x}{dz^2} = -\frac{qV_s}{W_b} \cdot \frac{z}{c_1 a_1^2} = -f \cdot \frac{z}{c_1 a_1^2}$$

$$\Rightarrow \frac{dx}{dz} = \left.\frac{dx}{dz}\right|_0 - f \cdot \frac{z^2}{2c_1 a_1^2} \tag{9}$$

$$\Rightarrow x = x_0 + \left.\frac{dx}{dz}\right|_0 \cdot z - f \cdot \frac{z^3}{6c_1 a_1^2} \tag{10}$$

From above, we can see that equation (3) is the case of letting the scaling factor $c_1 = 1$.

The 2nd case is the ion flying through the fringe region2 from the plates region to the drift region. See figure 7(b), the vertical field in fringe region2 can be simplified as:

$$E_x = \frac{2V_s}{a_1} \cdot \left(1 - \frac{z}{c_2 a_2}\right)$$

Then, the ion trajectory in the region2 is decided by the following:

8

$$\ddot{x} = \frac{d^2x}{dt^2} = -\frac{2qV_s}{m_i a_2} \cdot \left(1 - \frac{z}{c_2 a_2}\right) = \frac{d^2x}{dz^2} \cdot \left(\frac{dz}{dt}\right)^2 = \frac{d^2x}{dz^2} \cdot \frac{2W_b}{m_i}$$

$$\Rightarrow \frac{d^2x}{dz^2} = -\frac{qV_s}{W_b} \cdot \left(\frac{1}{a_2} - \frac{z}{c_2 a_2^2}\right) = -\frac{f}{a_2} + \frac{fz}{c_2 a_2^2}$$

$$\Rightarrow \frac{dx}{dz} = \left.\frac{dx}{dz}\right|_0 - \frac{f}{a_2} \cdot z + \frac{fz^2}{2c_2 a_2^2} \tag{11}$$

$$\Rightarrow x = x_0 + \left.\frac{dx}{dz}\right|_0 \cdot z - \frac{fz^2}{2a_2} + \frac{fz^3}{6c_2 a_2^2} \tag{12}$$

Equation (4) is the case where letting $c_2 = 1$.

C. Determination of Voltages on the secondary radial sweep plates

The secondary radial sweep plates steer the secondary charged ion beam to hit the vertical center of the analyzer entrance slit. Fig.8 shows the projection views of the radial sweep plates and an ion trajectory.
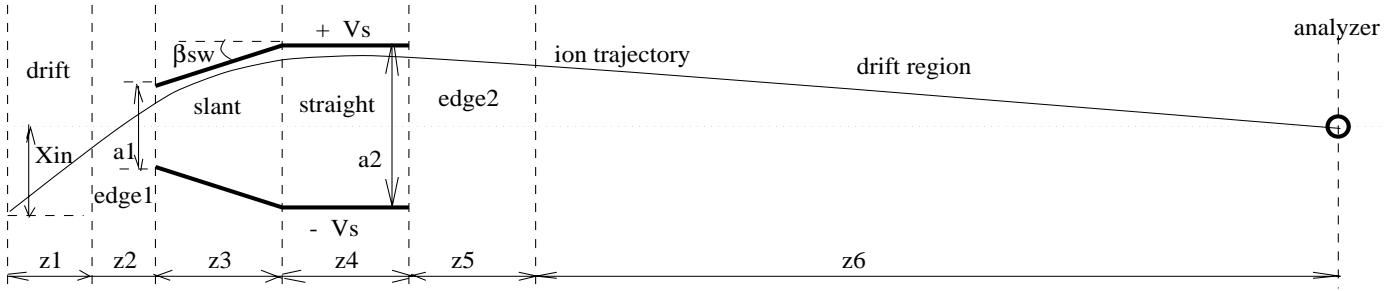

FIG. 8. Calculation regions of the radial sweep plates

In the figure, $z1$ is the length of a front drift region; $z2$ is the length of the front edge region $\sim a1$; $z3$ is length of the flared region; $z4$ is the straight region length; $z5 \sim a2$ is a fringe region; $z6$ is length of the drift region before the analyzer. We want to decide the voltage Vs that will be required to steer the trajectory to the vertical center of the analyzer. This is done by applying previous transfer equations (1)-(4) on the above regions. The final voltage needed is decided by the following if the incident position and angle are known:

$$f = \frac{A}{B} \tag{13}$$

where $f \equiv qVs/Wb$, and q is the charge of the ion (secondary charged); Wb is the beam energy.

$$A = Xin + (z_1 + z_2 + z_3 + z_4 + z_5 + z_6) * Vin \tag{14}$$

and

$$B = \left[\frac{z_2^2}{6a_1} + \frac{z_2 z_3}{2a_1} - \frac{z_3}{k} + \frac{1}{k}\ln\left(1 + \frac{kz_3}{a_1}\right)\left(z_3 + \frac{a_1}{k}\right)\right] + \left(\frac{z_4^2 + z_5^2}{2a_2} - \frac{z_5^2}{6a_2}\right) +$$

$$\left[\frac{z_2}{2a_1} + \frac{1}{k}\ln\left(1 + \frac{kz_3}{a_1}\right)\right](z_4 + z_5 + z_6) + \left(\frac{z_4 z_5 + z_4 z_6 + z_5 z_6}{a_2} - \frac{z_5 z_6}{2a_2}\right) \tag{15}$$

where $Vin = dx/dz|_0$ is initial slope of the trajectory; $k \equiv 2\tan(\beta_{sw})$.

D. Determination of Voltages on the secondary toroidal sweep plates

The secondary toroidal sweep plates steer the ion beam to the horizontal center of the analyzer entrance slit with zero toroidal incident angle. This is implemented by two pairs of plates. Fig.9 shows projection view of the secondary sweep plates and trajectory calculation regions.
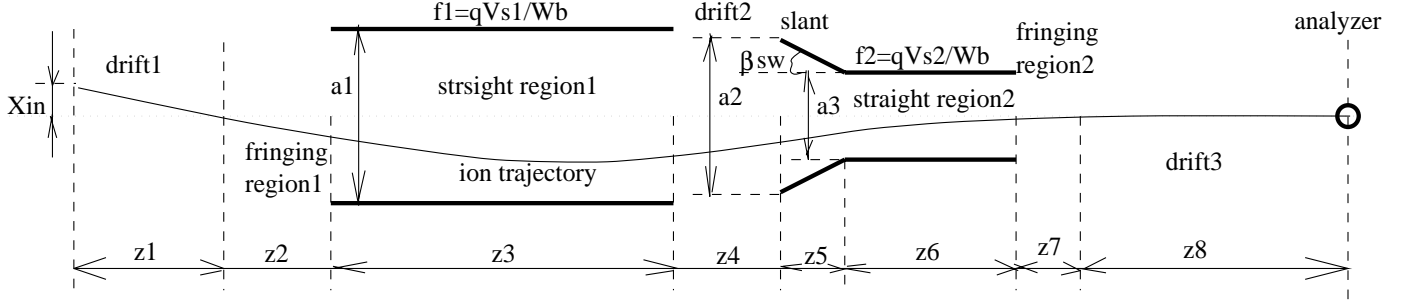

FIG. 9. Toroidal sweep plates and trajectory calculation

$z_1 - z_8$ have similar meanings as before. We want to find $f1$ and $f2$, which decide the voltages needed on the plates to satisfy our requirements. For simplicity, the region between two pairs is considered as a drift region. The voltages needed are decided by the following equation(s) if the incident position and angle are known:

$$\begin{bmatrix} f_1 \\ f_2 \end{bmatrix} = \begin{bmatrix} A_{11} & A_{12} \\ A_{21} & A_{22} \end{bmatrix}^{-1} \cdot \begin{bmatrix} -Xin - Vin * (z_1 + z_2 + z_3 + z_4 + z_5 + z_6 + z_7 + z_8) \\ -Vin \end{bmatrix} \quad (16)$$

where

$$A_{11} = -\frac{z_2^2}{6a_1} - (z_3 + z_4 + z_5 + z_6 + z_7) * \left(\frac{z_2}{2a_1} + \frac{z_3}{a_1} \right) + \frac{z_3^2}{2a_1} \quad (17)$$

$$A_{12} = \frac{z_5}{k} - \frac{z_6^2}{2a_3} - \frac{z_6 z_7}{a_3} - \frac{z_7^2}{2a_3} + \frac{z_7^2}{6a_3} - \frac{z5 + z6 + z7}{k} \cdot \ln\left(1 + \frac{kz_5}{a_2}\right) - \frac{a_2}{k^2} \cdot \ln\left(1 + \frac{kz_5}{a_2}\right) \quad (18)$$

$$A_{21} = -\frac{z_2}{2a_1} - \frac{z_3}{a_1} \quad (19)$$

$$A_{22} = -\frac{\ln\left(1 + \frac{kz_5}{a_2}\right)}{k} - \frac{z_6 + z_7}{a_3} + \frac{z_7}{2a_3} \quad (20)$$

In the above, $Vin = dx/dz|_0$ is the initial incident trajectory slope; $k = 2\tan(\beta_{sw})$. Therefore, we can decide the voltage on the straight plate (top) is $Vs1 = W_b \cdot f_1$, and voltage on the flared plate (top) is $Vs2 = W_b \cdot f_2$. The voltages calculated from above are a little bit overestimated, because of simplification made before.

E. Reducing edge (side) field effects with guard rings

When we design the sweep plates, we assume it's a 2-D problem with the width of the plate being infinite wide. But the width of the plate is always limited by the size of the vacuum chamber. Near

the tranverse edges, the field will no longer be uniform. Flux2d has been used to simulate the fringe fields. And guard rings are used to reduce the field nonuniformity at the sides.
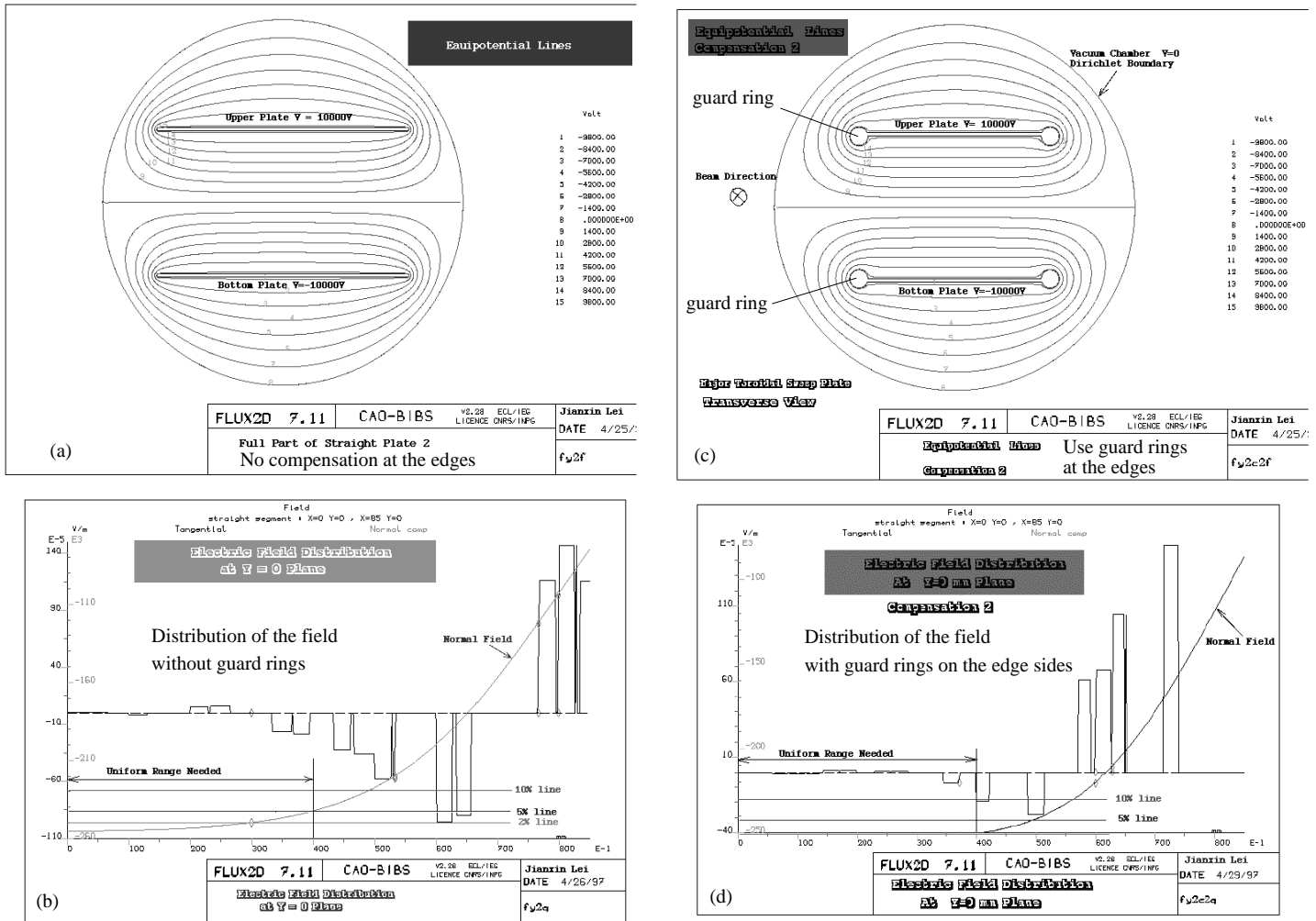

FIG. 10. Compensation of the edge field

Figure 10(a) shows a straight plate pair with the field distribution as shown in figure 10(b). Figure 10(c) shows the same plates but with guard rings at the transverse sides. The plates with guard rings also have smaller width. However, from figure 10(d), which shows the field distribution of case (c), we can see that the uniform field region is larger than that shown in figue 10(b). The uniform region size needed is decided by the transverse motion range of the ion beam. Therefore, not all the plates need guard rings at their sides if the transverse motion range is small and the openning of the plates is small too. Geometry of the primary and secondary sweep plates as shown in appendix F and G satisfy both trajectory and uniformity requirements.

F. Primary sweep plates geometry and parameters

Figure 11 shows the parameters and geometry of the primary sweep plates and guard rings configuration.
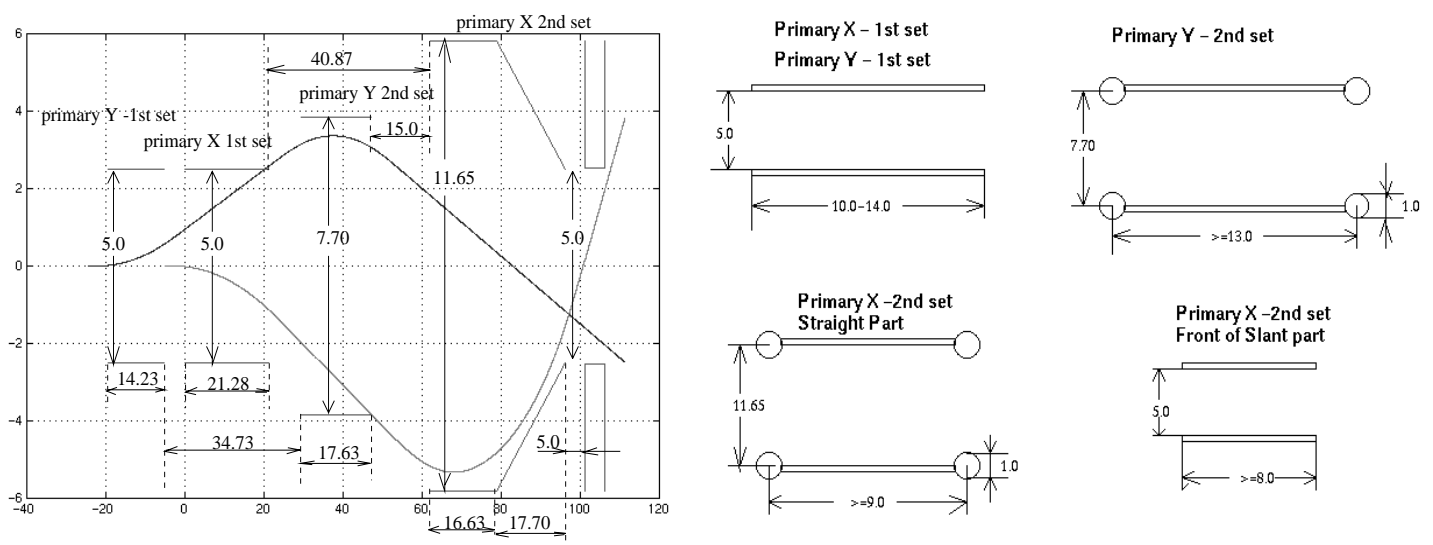
FIG. 11. Parameters and geometry of the primary sweep plates designed: (a) length of each plate and the primary system configuration; (b) cross section configurations, guard rings and width of each plate

G. Secondary sweep plates geometry and parameters

Figure 12(a) shows the parameters and geometry of the secondary sweep plates and its toroidal position for edge diagnostics. Figure 12(b) shows the parameters and geometry of the secondary sweep plates and its toroidal position for core diagnostics.

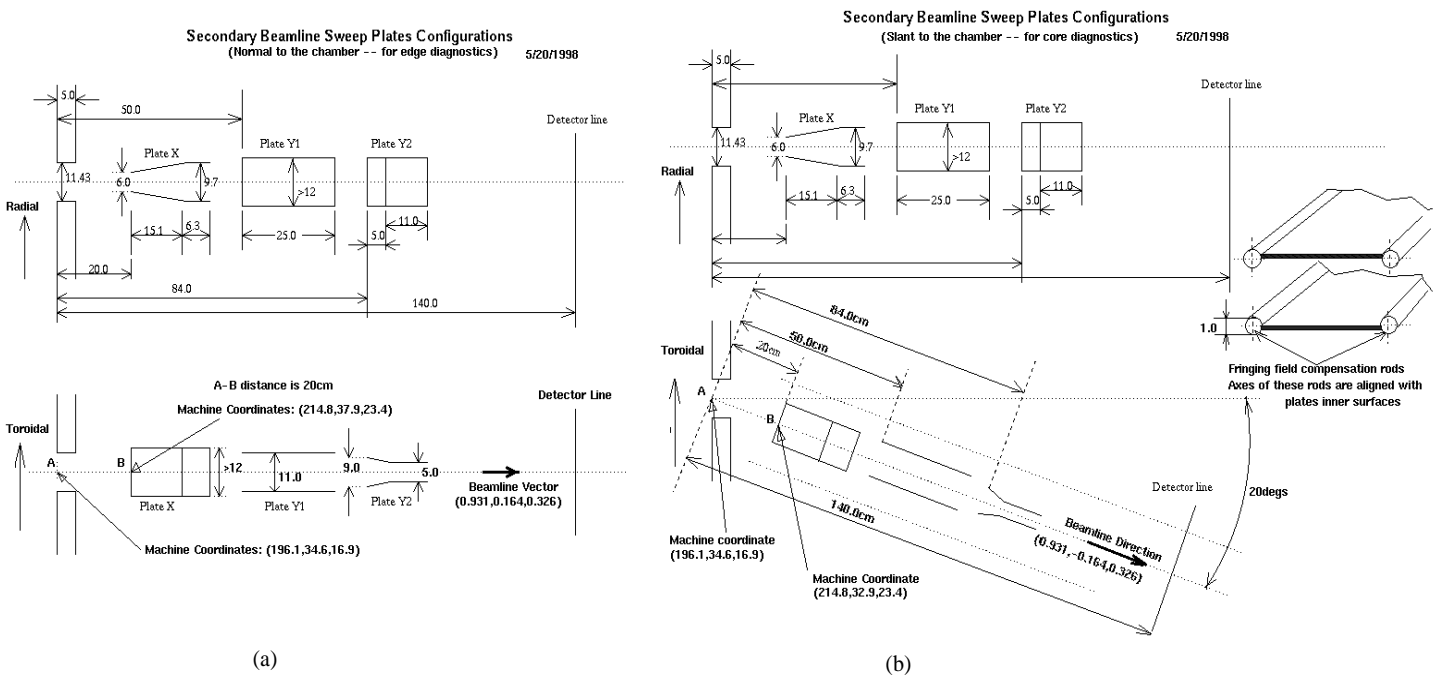(a)   (b)

FIG. 12. Parameters and geometry of the secondary sweep plates designed and its position: (a) for edge measurements; (b) for core measurements

Figure 13 shows a 3D view of the arrangement of the sweep system to perform edge and core diagnostics. Also refer to figure 4 which shows top views of those arrangements.
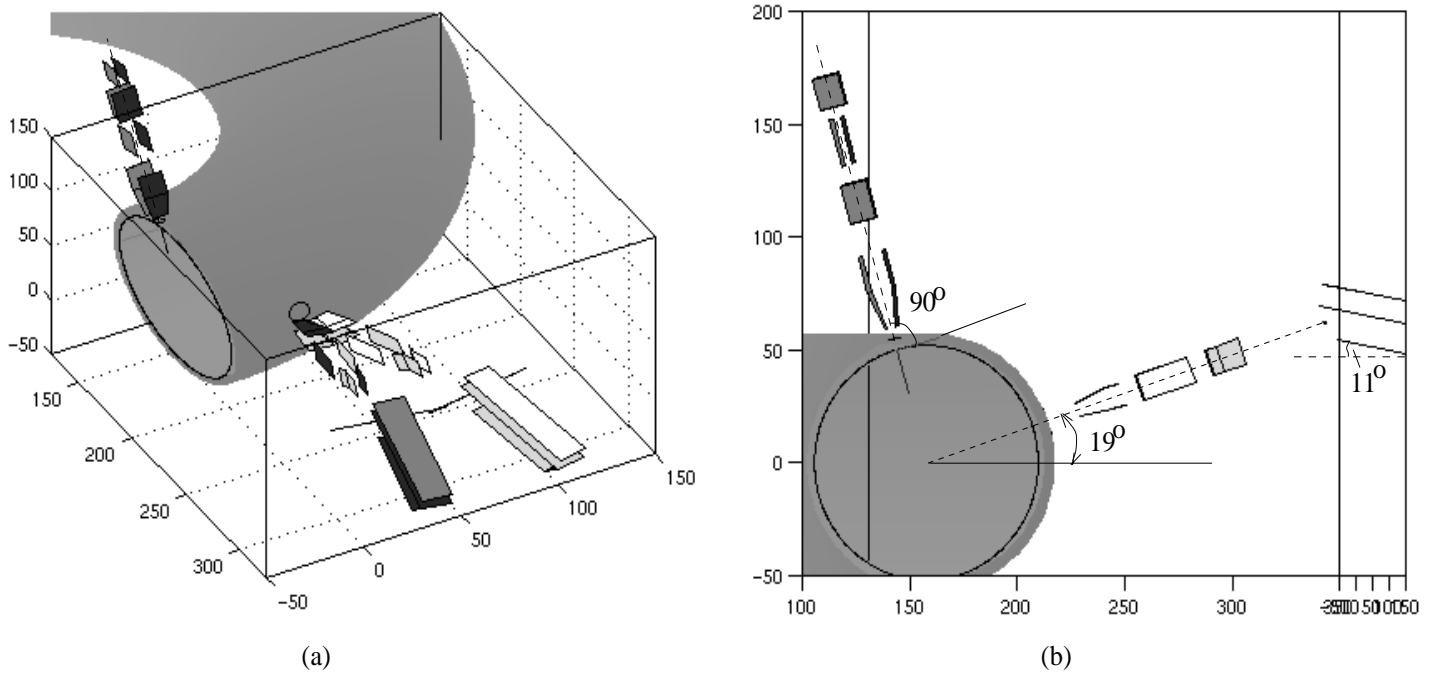
12

(a)	(b)

FIG. 13. A 3D view of the beamlines arrangement for edge and core diagnostics

H. Trajectory calculations in the MST-HIBP

There are two ways to calculate beam trajectory in the sweep system. The 1st is to use previous eqs. (1)-(4). The 2nd is to find electric field in the sweep region with flux2D/3D, and use Runge-Kutta method to solve the trajectory problem. Trajectories in the MST plasma are calculated from a modified version of a fortran code that has been used for about 20 years. This fortran code can produce such information as secondary birth position, sample volume shape and size, incident position and angles at the detector plane, etc. The core of the code was given by Steve C. Aceto, and Ying Dong did most of the modification to make it MST special. The author has modified Dong's version in order to make it compatable with matlab programs. The idea of crossover design was first proposed by prof. Crowley. The author developed the modified model to treat fringing field effects. There is also a matlab trajectory code which was originally written by prof. Connor using Euler method and has been modified by the author to calculate trajectories in the plasma. Matlab programs are easily to be modified to produce information of specific interest and to plot the results. But the sample volume information corresponding to the given detector position is calculated by the fortran code because of speed.

The process of trajectory calculation is: (1) Primary beam: set voltages range on each sweep pair (refer to figure 11(a)): the upper and down limit of these voltages are: -4 - +4 kV on the primary X & Y 1st sets; -10 - +10 kV on the primary Y 2nd set; -20 - +20 kV on the primary X 2nd set. Use modified model or flux2D results to calculate the primary beam trajectory. The output results include injection position and angle information at the entrance port. (2) Take those outputs from the primary calculation as inputs to the fortran code to generate primary and secondary trajectories in the plasma. Outputs from the fortran code are information of incident position and angle at the (virtual) detector plane. (3) Secondary beam: voltages on the secondary sweep plates are determined by the equations in the appendix C and D, with initial incident conditions being the outputs from the fortran code. Fields from flux2D simulations can be used to check the results.

13

Average computer time needed to generate a full scale trajectory on a sun sparc is 5 - 10 sec. if using the modified model. More time is needed if using flux2D fields. The average difference between the modified model and flux2D is below 5% for the primary trajectory and is very small for the secondary. One disadvantage of using flux2D is that the geometry of the sweep plates has to be designed and known first, and can not change during the calculations. The modified model doesn't have this restriction.

There are some other matlab programs used to produce projections of the primary or secondary on the vacuum chamber or an arbitrary plane, to plot MST B fields, etc. All these including the fortran code will be combined together in future. Some detailed explanations of these programs have been written by the author.

In the trajectory calculations, the MST plasma current has been set at 350 kA, and average B field configuration (average state between pre-sawtooth and post-sawtooth) has been used.

I. Looking for proper beamlines positions and rotation angles

In the previous sections, both beamlines position has been decided by the diagnostic requirement and preliminary trajectory calculations. We can see that the edge and core regions can be measured respectively by putting the secondary beamline at two different positions. In the previous calculations, we did try a lot to play with both primary and secondary beamlines (including re-positioning, tilting, rotating, etc.) to find a proper configuration of the beamlines. However, for simplicity, we didn't exhaust all possibilities. In this section, we'll input a little bit more effort to find a proper configuration of the beamlines. The goal is to cover more MST plasma with our ion beam but with less motion of the beamlines (especially the secondary beamline). Ideal situation is both the primary and secondary beamlines are fixed, but radius scan is achieved by just sweeping the voltages on the sweep plates and probably stepping the beam energy during 2-3 shots. The matlab programs for the primary and secondary sweep plates design have capability of tilting and rotating the beamlines in the calculation.

This work is in process now and will be updated if necessary.

J. Determination of the magnets structure position and openning size

It is believed that magnetic field can be used to reduce plasma loading effect. In order not to block our ion beams, it's necessary to find a proper location of this magnets structure. For the primary beamline, the magnets should be put at the position between the last radial sweep plates and the entrance port. This is the major topic of this section.

Because the sweep point in the radial direction is different from that of the toroidal direction, we have to put the magnets structure around the radial sweep point which is between the last plates and the entrance port. As in real case the sweep point moves along the axis in a certain region because of different sweep angles, we have to do some calculations to decide this range. Figure 14(a) shows the trajectories in the radial plane, and 14(b) shows that in the toroidal plane. Both modified model and flux2D results are used to give us more insight into the motion of the sweep points.
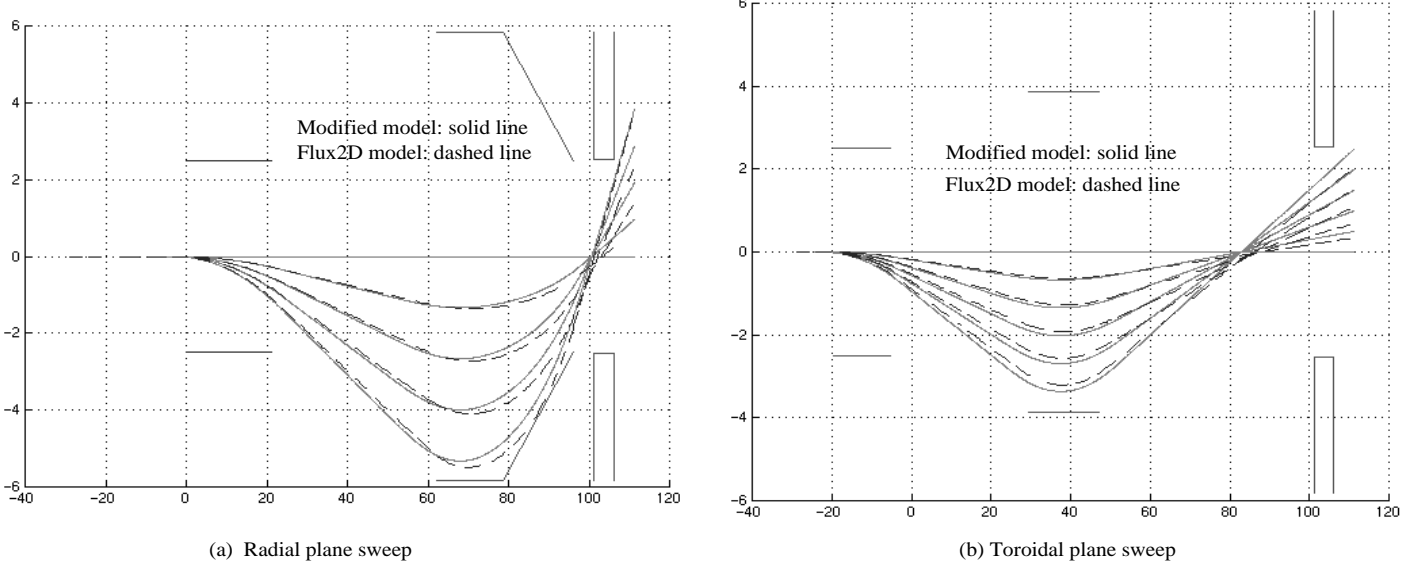
(a) Radial plane sweep (b) Toroidal plane sweep

FIG. 14. Sweep points in the (a) radial plane; (b) toroidal plane

Modified model will give us a fixed sweep point, while flux2D model will not. Table 1 list the calculated cross axis positions at different sweep angles. Note that in the coordinate system of that shown in figure 14, the entrance port is sitting between 101.2 - 106.2 cm.

TABLE I. Cross axis positions on the radial and toroidal planes

	On the radial plane			On the toroidal plane	
Angle	Modi. Model	Flux2D	Angle	Modi. Model	Flux2D
0°	—-	—-	1°	82.85 cm	87.98 cm
0°	100.67 cm	103.45 cm	2°	82.85 cm	87.59 cm
10°	100.67 cm	103.05 cm	3°	82.55 cm	87.18 cm
15°	100.67 cm	102.28 cm	4°	82.55 cm	86.05 cm
20°	100.67 cm	101.03 cm	5°	82.55 cm	85.19 cm

From table 1, we can see that our magnets structure should be put at the axis position of around 102.2 cm, which is 4 cm away from the plasma. The openning size of this slit can be decided by the beam size used and toroidal displacement of the beam at 102.2 cm axis position. Table 2 shows toroidal displacements information around the effective radial sweep point calculated from the modified model.

TABLE II. Toroidal displacement range of the beam around the effective radial sweep point

Axis position	Toroidal displacement
101.5 cm	1.63 cm
102.0 cm	1.68 cm
102.5 cm	1.72 cm
103.0 cm	1.76 cm
103.5 cm	1.80 cm

If we assume that the ion beam that will be used is about 1.0 cm in diameter, the openning size of our magnets structure should be at least $2*(1.76+0.5) = 4.52$(cm) in width, where the length of this structure is assumed about 1.5 cm (along the axis).

Table 3 shows radial displacements information around the effective radial sweep point calculated from both the modified and flux2D models.

TABLE III. Radial displacement range of the beam around the effective radial sweep point

Axis position	Modified model					Flux2D model				
	101.5 cm	102.0 cm	102.5 cm	103.0 cm	103.5 cm	101.5 cm	102.0 cm	102.5 cm	103.0 cm	103.5 cm
20°	0.25 cm	0.45 cm	0.62 cm	0.80 cm	0.99 cm	0.12 cm	0.30 cm	0.49 cm	0.68 cm	0.87 cm
15°	0.18 cm	0.33 cm	0.47 cm	0.61 cm	0.74 cm	-0.20 cm	-0.08 cm	0.07 cm	0.20 cm	0.33 cm
10°	0.13 cm	0.22 cm	0.32 cm	0.40 cm	0.49 cm	-0.25 cm	-0.17 cm	-0.08 cm	0 cm	0.08 cm
5°	0.07 cm	0.11 cm	0.14 cm	0.20 cm	0.25 cm	-0.16 cm	-0.12 cm	-0.08 cm	-0.04 cm	0 cm

Assuming that the ion beam is 1 cm in diameter as before, for a conservative design, the height of the magnets slit should be at least $2*(0.8+0.5) = 2.6$(cm).

Therefore from above analysis, we can decide that the openning of this magnets structure should be about $(H)2.6 \times (W)4.52 \sim 11.8 cm^2$. The location of this structure should be around 4 cm away from the plasma and therefore inside the entrance port.

For the secondary beamline, similar magnets mitigation structure should be used too. Difficulty there is that the secondary beam will cover the whole front openning area of the radial sweep plates. The magnets slit would be about 6 cm in height, and 11.4 cm in width, which is not totally impossible is combined with a fine metal mesh screen. Otherwise, by sacrificing some secondaries and sample volumes, a smaller openning size is applicable if confirmed by some more calculations.